Proceedings of the 8th World Congress on Momentum, Heat and Mass Transfer (MHMT'23)
Lisbon, Portugal – March 26 – 28, 2023
Paper No. ICMFHT 133
DOI: 10.11159/icmfht23.133

Experimental and Numerical Study of a Cryogenic Ball Valve Using Liquid Nitrogen

Maria Teresa Scelzo [1], Maria Faruoli[1], Hubert Lejeune[2], Sandra Varin[2], Jorge Pinho[1]
[1]von Karman Institute for fluid dynamics
72 Chaussée de Waterloo, B-1640 Sint-Genesius-Rode, Belgium
scelzo@vki.ac.be; faruoli@vki.ac.be; pinho@vki.ac.be
[2]CETIM Centre Technique des Industries Mécaniques
74 Rte de la Jonelière, 44300 Nantes, France
hubert.lejeune@cetim.fr; sandra.varin@cetim.fr

Abstract – This paper addresses the experimental and numerical study of a cryogenic ball valve using liquid nitrogen as working fluid. Experimental tests were performed in the Cryoline facility at the von Karman Institute for Fluid Dynamics (Belgium) in collaboration with Centre Technique des Industries Mécaniques (France). Mass flow rate, pressure, and temperature measurements were performed during the tests, and synchronized with high-speed flow visualization. Subcooled liquid nitrogen was ensured upstream the valve. Three different valve apertures, with different back pressure values, enabled both fully liquid and two-phase flow conditions downstream the valve. Besides the flow regime and the hydraulic performance, the valve stem temperature was monitored during the tests and the subsequent accelerated transient warming of the cryogenic line. In parallel, isothermal CFD simulations were performed in OpenFoam using a standard cavitation model. Results in single and two-phase flow conditions are compared to the experimental findings.

Keywords: cryogenic ball valve, cavitation model, valve stem temperature

1. Introduction

According to Stratview Research (2022), the cryogenic valve market will likely have a compound annual growth rate (CAGR) of 4.8% in the next five years. Increasing trade of LNG and LH2 has led to high demand for the storage and transportation of cryogenic fluids, augmenting the need for cryogenic valves. This market growth requires further research and deeper development of guidelines tools to support the design and sizing of such devices.

The flow through a restriction, such as a valve, undergoes different regimes depending on the pressure drop across the restriction, as shown in Figure 1 (adapted from [1]). Three distinct regions can be appreciated:

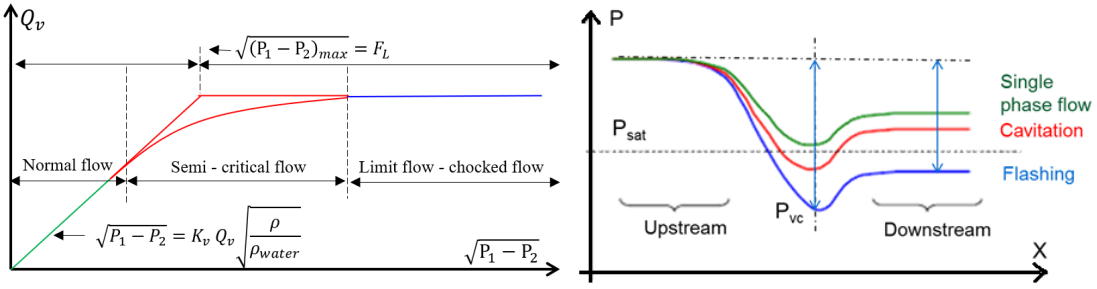

Figure 1: Hydraulic performance of a flow restriction (valve), adapted from [1]

i) In the normal flow region, the volumetric flow rate (Q_V) is proportional to the square root of the pressure drop ($\sqrt{P_1 - P_2}$) across the restriction, according to the flow coefficient Kv reported in Eq (1):

$$K_v = \frac{Q_V}{\sqrt{P_1 - P_2}} \sqrt{\frac{\rho_1}{\rho_{water}}} \tag{1}$$

where ρ_1 is the inlet density. Kv corresponds to the slope of the valve hydraulic curve, and it defines the volumetric flow rate of water at ambient temperature, passing through a restriction when a pressure difference of 1 bar acts across its body. The pressure downstream the valve is always higher than the saturation pressure having a minimum at the vena *contracta* position (P_{VC}). ii) In the semi-critical region, the flow rate increases with the increment of the square root of the pressure

drop but not linearly, since phase change appears downstream the restriction. Finally, in the iii) limit flow or choked region, the mass flow rate is choked and can no longer increase despite pressure difference continues to increase.

The Liquid Recovery Factor FL , calculated as in Eq.s (2), is a parameter that provides an indication on the pressure evolution across the restriction. Graphically, it corresponds to the intercept between the normal flow linear curve and the choked flow condition: where the maximum pressure drop and vaporization across the restriction is achieved.

$$F_L = \sqrt{\frac{(P_1 - P_2)_{max}}{(P_1 - P_{VC})}} \; ; \; P_{VC} = F_F P_{sat} \; ; \; F_F = 0.96 - 0.28\sqrt{\frac{P_{sat}}{P_{crit}}} \tag{2}$$

As P_{VC} is always lower than the downstream pressure, F_L is always lower or equal to 1. P_{VC} is generally not known and extremely difficult to measure and localize along the restriction body. A possible approach is to assume P_{VC} equal to a fraction of the upstream saturation pressure through the Liquid Critical Pressure Ratio Factor F_F, that can be calculated as proposed by Stiles [2] and reported in Eq.s (2). The relations given in Eq. (1) and Eq.s (2) are included in the recommendations of IEC 60534 [3] for the sizing of control valves.

This work presents the experimental and numerical investigation of the flow through a cryogenic ball valve according to the flow regimes and with the correlations described earlier. Moreover, it shows an analysis of the temperature gradient across the valve stem during the cryogenic experiments and during the body warming up, accelerated by gas nitrogen (GN2) at different valves of flow rates.

2. Experimental facility and procedure

The experiments were performed in the Cryoline facility at the von Karman Institute (VKI) for fluid dynamics, which is illustrated in Figure 2. A precedent work by the same research group [4] has been performed in the same experimental facility to test a cryogenic valve used in launch vehicle liquid propulsion systems.

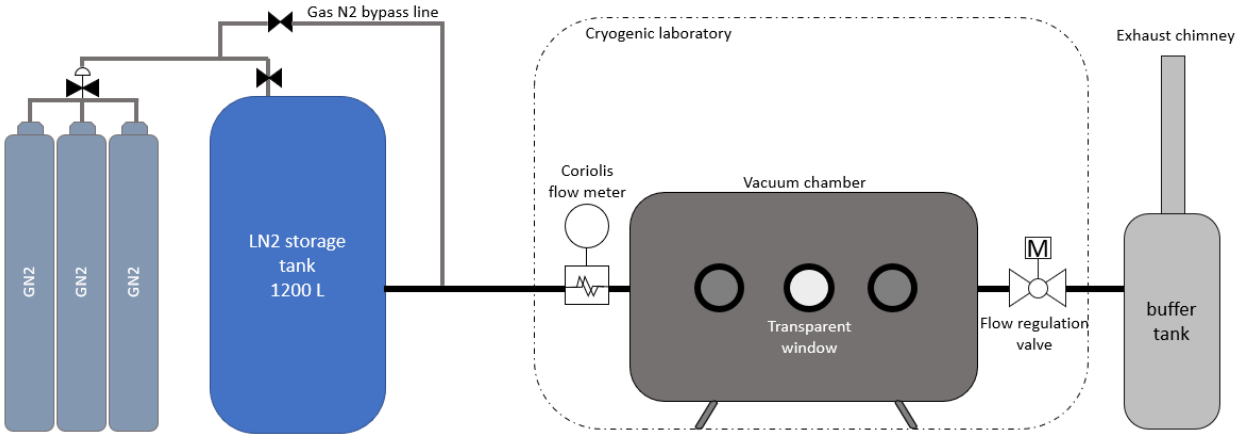

Figure 2: VKI Cryoline facility layout

Liquid nitrogen (LN2) is stored outside the cryogenic laboratory in a 1200 L storage tank. The volume is large enough to ensure a mass flow rate in the test section as high as 0.6 kg/s for 15 minutes. Next, the liquid travels in an insulated pipe to the cryogenic laboratory, where a Coriolis flow meter measures the liquid mass flow rate upstream of the test section. The test section is mounted inside a vacuum chamber and includes a DN15 stainless-steel pipe with a thickness of 0.5 mm and two quartz windows for the flow visualization, one upstream and one downstream of the valve. To prevent optical distortions linked to the channel round shape, the quartz pieces have a circular internal section and a rectangular external section. The selected testing valve is a cryogenic 30° V-control ball that offers a high flow regulation sensitivity starting from an opening angle of 25°. A manual handle drives this regulation valve. Downstream of the test section, outside the vacuum chamber, a

DN40 ball valve, motorized and with pneumatic actuation, regulates the back pressure and hence the mass flow rate during the experiments. Finally, the nitrogen is vented outside the laboratory via the external chimney.

Beyond the LN2 testing conditions, a bypass line has been added from the gas bottles to the nitrogen line to perform tests with warm GN2 at controlled pressure.

The test section schematic is reported in Figure 3, where LN2 flows from the left to the right.

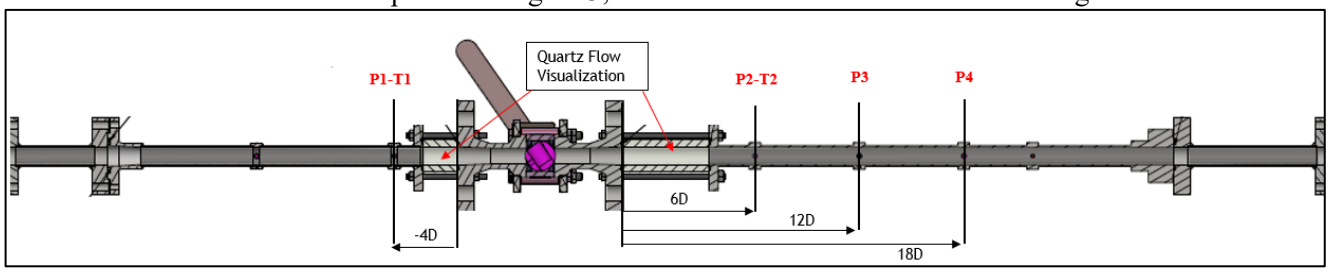

Figure 3: Test section schematic.

LN2 thermodynamic conditions are measured with temperature and pressure sensors mounted at the same location upstream (P1,T1) and downstream of the valve (T2,P2). LN2 temperature is measured with cryogenic silicon diodes (DT-6708-SD by Lakeshore) at a sampling frequency of 50 Hz. The electric resistance signal is acquired by a 218S acquisition monitor and converted in temperature using the built-in calibration suitable for the used silicon diode. The same sensors are glued on the valve stem to monitor the valve body temperature during the tests. The LN2 pressure, valve pressure drop and flow fluctuations are measured with Kulite cryogenic sensors (CTL-190SM-17 BARA) with acquisition frequency of 100 kHz. The full-scale sensor output signal of 100 mV is amplified up to maximum 10 V via Fylde FE-H379-TA. The LN2 mass flow rate is measured with a Coriolis flow meter (Yokogawa RCCS38 DN40). Flow visualization is performed with a Dantec Speedsense V2012 high speed camera through the window downstream the valve. The frame resolution selected is 896 pixels x 304 pixels, exposure time between 30 and 40 microseconds, and acquisition frequency equal to 14 kHz. The camera mounts a Nikon Macro 105mm objective.

The experimental procedure shown in Figure 4 (for valve aperture equal to 90°) consists of three steps: the line chill down (0<t<900s), the steady state testing time (900<t<2000s), the line warmup (2000<t<7000s). The last phase can be performed at no flow conditions or accelerated with warm GN2 at controlled pressure travelling via the GN2 bypass line (as shown in Figure 1). In this way, the warm-up time decreases to 2000s with GN2 at 2 bar, and to 1350s with GN2 at 5 bar.

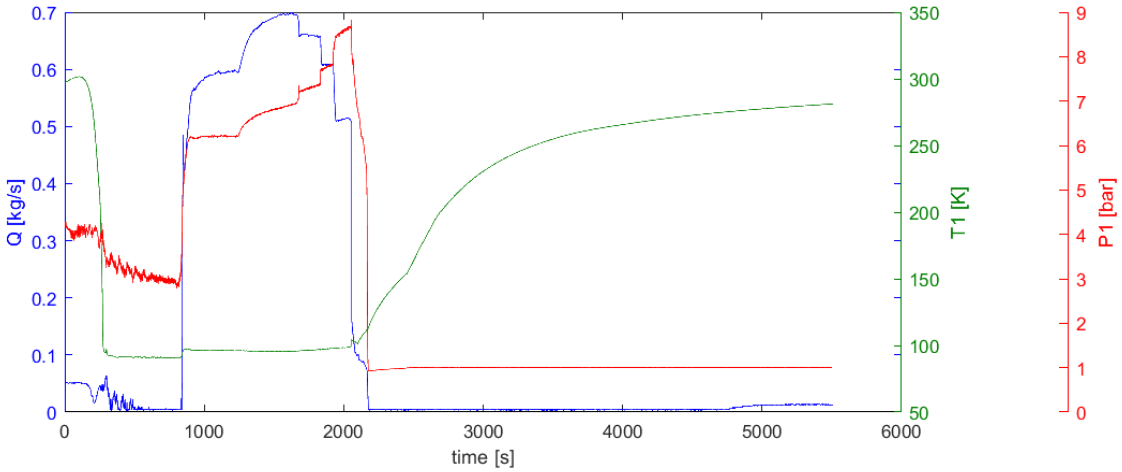

Figure 4: Typical test history in terms of mass flow rate (Q), inlet temperature (T1) and pressure (P1)

3. Numerical model and setup

The cavitation phenomenon is simulated with interPhaseChangeFoam, a multi-phase solver of OpenFOAM that uses the volume of fluid method, and already includes different models to simulate the presence of the phase change. The solver uses an incompressible formulation of the mass conservation (Eq.(3)) and momentum conservation (Eq.(4)) equations. Hence, the properties of the fluid and the vapor phases are considered constant, and they are calculated according to the reference experimental LN2 inlet temperature. Moreover, no energy transport equation is solved. This represents a strong simplification of the problem, since it has been proved in a previous work [5] that the variation of the thermo-physical properties of the materials can influence the results of the simulation. Despite this, it has been decided that for this application, the incompressibility hypothesis is acceptable since from the experiments no large temperature gradients are observed. Moreover, the solver includes the void fraction transport equation reported in Eq.(5).

$$\frac{\partial \rho_m}{\partial t} + \nabla \cdot (\rho_m \boldsymbol{u}) = 0 \tag{3}$$

$$\frac{\partial \rho_m \boldsymbol{u}}{\partial t} + \nabla \cdot (\rho_m \boldsymbol{u}\boldsymbol{u}) \frac{\partial \rho_m}{\partial t} + \nabla \cdot (\rho_m \boldsymbol{u}) = 0 \tag{4}$$

$$\frac{D}{Dt}\rho_v \alpha_v + \rho_v \alpha_v \nabla \cdot (\boldsymbol{u}) = R_{source} \tag{5}$$

The void fraction source term (R_{source}) models the change of phases due to cavitation. This term is modelled with the Schnerr-Sauer approach as shown in Eq. (6), which is based on the bubble dynamic theory and presents a high accuracy level [6]. More specifically, it considers as coefficients the number of bubbles that are created in the liquid once the pressure decreases below the saturation pressure, and the dimension of the bubbles created during cavitation as in Eq. (7). This model requires specific coefficients for LN2 such as the parcels density ρ_m, *n=1.6e8*, and the $C_{c|v}$*=1* [7].

$$R_{source} = C_{c|v} \frac{\rho_l \rho_v}{\rho_m} \alpha_v (1 - \alpha_v) sgn\left(p - p_{vap}\right) \frac{3}{R_b} \sqrt{\frac{2}{3} \frac{\left|\left(p - p_{vap}\right)\right|}{\rho_l}} \tag{6}$$

$$R_b = \left(\frac{1 - \alpha_v}{\alpha_v} \frac{3}{4\pi} \frac{1}{n}\right)^{\frac{1}{3}} \tag{7}$$

The numerical domain is extended upstream and downstream of the valve location by 4D and 8D respectively. The computational grid, generated using the utility snappyHexMesh of OpenFOAM, is an unstructured mesh with mostly hexahedral elements. Specific zones are further refined such as the volumes upstream and downstream of the valve. A mesh independence analysis has been carried out, obtaining a final mesh composed of about 4.2. millions of cells for the 55° opening. Figure 5 shows some details of the grid for the opening identified as 55°.

The inputs required from the experiments are the total pressure at the inlet section and the static pressure at the outlet section, chosen to have a more stable convergence of the problem. Moreover, a fully liquid condition simulation is used to initialize a case where two-phase flow downstream the valve is expected in order to enable faster convergence of the cases in cavitating conditions.

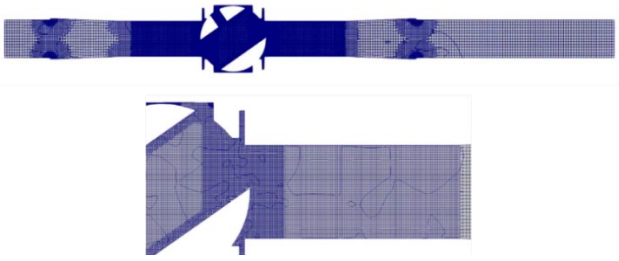

Figure 5:Computational grid domain

4. Experimental results and comparison with the CFD

Figure 6 shows the experimental and numerical results for the three valve apertures tested and a few exemplary video frames used to identify the flow regime downstream of the test section. In the plots, the circular markers correspond to fully liquid conditions downstream of the valve, whereas the triangular markers denote the appearance of two-phase flow. Besides, the full markers represent the experiments, and the empty markers show the CFD calculation results. The dashed line is the theoretical linear proportionality between the volumetric flow rate through the valve and the pressure drop across it, as declared by the valve manufacturer via the Kv. In the video frames, the flow direction is from left to right, the clear regions correspond to the liquid phase, and the darker regions denote the presence of the vapor phase.

In Figure 6, in some cases, circles (single-phase points) and triangles (two-phase flow points) markers have very similar pressure drop values and mass flow rate values. This is because these tests are conducted at different inlet pressures (ranging from 7.0 to 9.7 bar); thus, a similar pressure drop may correspond to different flow regimes. In Figure 6(top), it is also interesting to notice the flow regime transition between liquid flow (p8) and vaporous flow (p5). As the flow rate diminishes (going from point p5 to p8), the flow visualization frame shows the vaporous front receding from far downstream (right part of the video frames) towards the region closer to the valve, until it disappears, and the fluid becomes liquid.

In fully liquid conditions, the CFD results match the experimental ones. Hence the prediction of the K_v is very close to the experimental value, as reported in Table1. Concerning the two-phase flow appearance, it can be noted for the cases of 55° and 70°, the flow rate seems to have reached a constant value, as expected from the literature (see Figure 1). The differences with the experiments might be due to the isothermal hypothesis in the numerical simulations, which imposes a constant value for the saturation pressure, whose value should change due to the temperature variation in the domain. This assumption might also affect the calculation of the F_L from the numerical results. According to the IEC Standard 60534 [2], the evaluation of F_L should be done with consequent tests at constant inlet pressure, reducing the pressure drop to 90% of the one recorded in the first test. If the flow rate in the second test is within 2% of the flow rate in the first test, this flow rate should be taken as the maximum flow rate. Since the experiments are performed at varying inlet pressure due to the experimental procedure and the facility working principle (as shown in Figure 4), the evaluation of the F_L might be affected. Hence, it is expected that the actual value of F_L is lower than the one reported in Table 1.

Table 1: Experimental and numerical values for K_v and F_L

Valve aperture	K_v, experimental $[m^3\ h^{-1} bar^{-1/2}]$	K_v, numerical $[m^3\ h^{-1} bar^{-1/2}]$	F_L – experimental [-]	F_L – numerical [-]
90°	2.52 ± 0.06	*2.51*	0.74 ± 0.04	*0.81*
70°	1.30 ± 0.03	*1.27*	0.93 ± 0.04	*0.72*
55°	0.68 ± 0.02	*0.59*	1.11 ± 0.05	*0.93*

Finally, Figure 7 shows the void fraction field extracted from the numerical simulations (left) in comparison with one exemplary video frame from high-speed imaging (right) for the test p6 at 55° aperture, reported in Figure 6 (top). The blue zone in the numerical field denotes the presence of minimum 0.5 gas fraction. Although the quantitative comparison of the void fraction is left for the future perspectives of this work, the numerical simulations retrieve the highly vaporous regime at the outlet of the valve and the pressure recovery, with consequent liquid re-formation, further downstream the pipe. Nevertheless, it is worth noticing that when the pressure outlet boundary condition, imposed equal to the experimental one, is close to or below the saturation pressure, the void fraction is, in some cases, clearly overestimated.

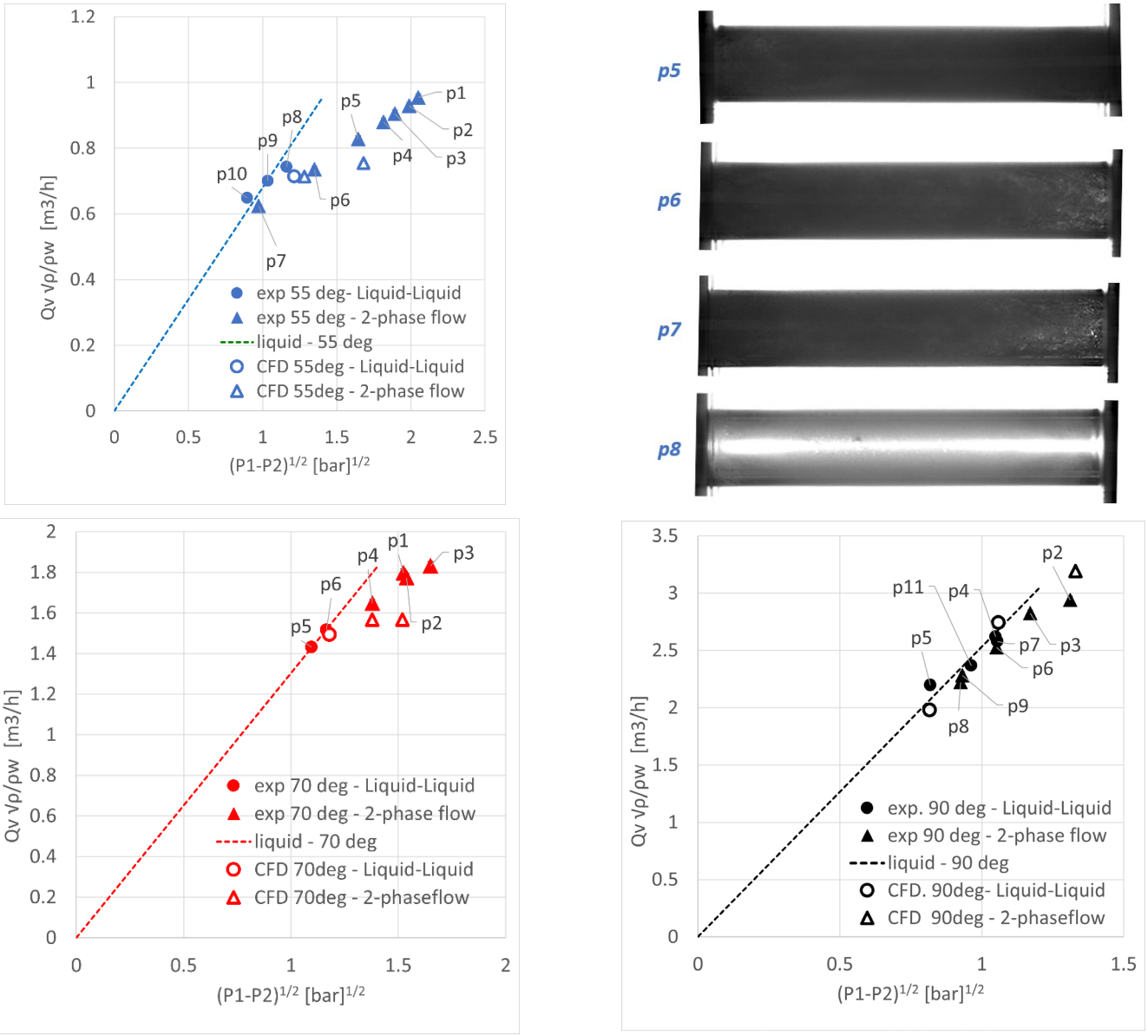

Figure 6: Hydraulic performance map and exemplary video frames for the experiments at valve aperture equal to 55° (top), 70° (bottom left) and 90° (bottom right). Comparison between experimental data (full markers) and CFD results (empty markers), for fully liquid conditions (circles) and two-phase flow conditions (triangles) downstream the valve.

Figure 7: Test p6 at 55° aperture: (right) void fraction field from CFD simulation (left) video frame from high-speed imaging.

5. Valve stem temperature evolution

During the tests, the valve temperature is measured by means of three silicon diodes (same kind used for the flow flow measurement), as shown in Figure 7(a). In first approximation the valve stem is modelled as a metallic bar, for which which the 1D transient conduction equation reported in Eq. (8) describes its temperature evolution over time.

$$\frac{\partial T_{valve}}{\partial t} = \frac{k}{c\rho}\frac{\partial^2 T_{valve}}{\partial x} \tag{8}$$

In Eq.(8), k, c and ρ are the thermal conductivity, specific heat, and density of the valve stem, that for this simplified approach is taken as stainless steel AISI316 at 100 K. Referring to Figure 8(a), x=0 corresponds to the stem part close to the liquid nitrogen flow, and x=L corresponds to the other extremity of the valve stem, in contact with the vacuum chamber atmosphere. The continuous lines in Figure 8(b) show the stem valve temperature measured over time. In this case, the warm-up is performed with GN2 at approximately 5 bar. The position T3, very close to the nitrogen flow, follows the behaviour of the fluid temperature, and the position T5 remains close to room temperature. Hence, in first approximation, at both extremities constant temperature is applied as boundary condition: at x=L, T= temperature of the vacuum chamber ($T_{chamber}$) and at x=0, T=temperature of the fluid. During chill-down and steady testing time, temperature of the fluid is T1 whereas during the accelerated warm-up, the GN2 temperature is estimated with the energy equation reported in Eq. (9).

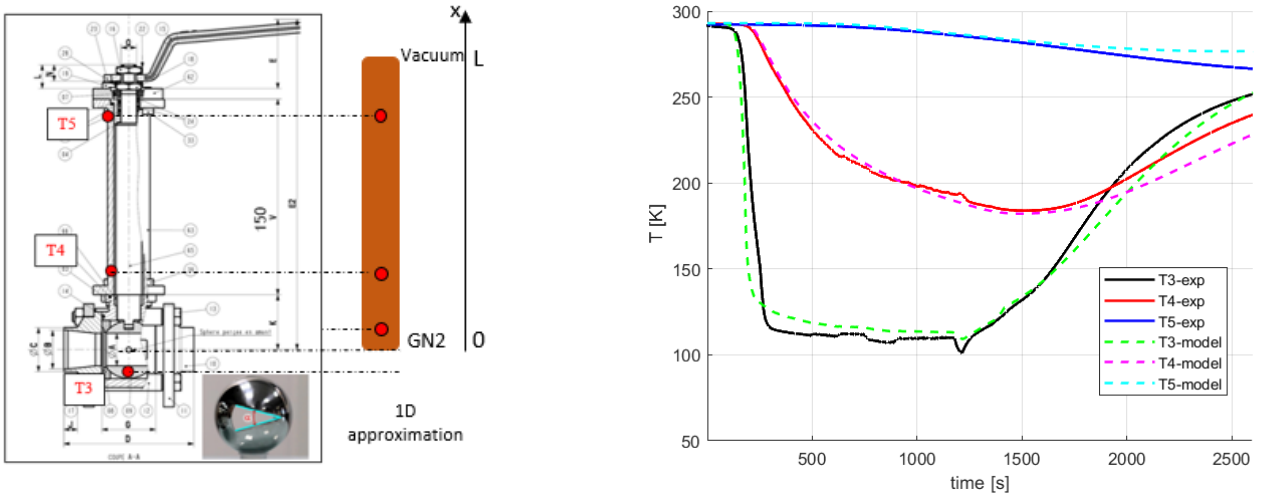

(a) (b)

Figure 8: (a) Temperature measurement position on the valve stem and simplified 1D computational domain (b) Comparison between experiments and model

$$\rho c\frac{\partial T_{gas}}{\partial t} + \rho cU\frac{\partial T_{gas}}{\partial x} = h\left(T_w - T_{gas}\right)\frac{2}{R} \tag{9}$$

In Eq.(9), the values of ρ and c are constant, and R is the pipe radius. The value of flow velocity U is calculated considering that the valve during the accelerated warm-up is characterized by the same K_v value than the liquid flow. Moreover, the heat transfer coefficient h derives from Dittus-Boelter correlation for Nusselt number in turbulent pipe flows [8]. The value of T_w (the wall temperature) is calculated as in Eq (10),

$$c_w\rho_w s_w\frac{\partial T_{wall}}{\partial t} = h\left(T_w - T_{gas}\right) + h_{vacuum}(T_w - T_{chamber}) \tag{10}$$

where the values of ρ_w and c_w are referred to the pipe material at 100K, s_w is the pipe thickness, h_{vacuum} is taken equal to 5 W/m^2K and $T_{chamber}$ is equal to 297 K.

The comparison between temperature measurements on the valve and the model is shown in Figure 8(b). The model (dashed lines) can predict within an overall 15% deviation the chill down procedure (0<t<400s) when the temperature decreases from 300K to ~100K, and the testing time (400<t<1200s), in which the flow temperature (hence the valve temperature) changes due to the pressure change in the line. It is possible to see that the position T3 is extremely sensitive to the fluid temperature change, whereas this is dampened for positions far from the fluid (T4). This suggests that the boundary conditions are well chosen. The prediction worsens during the accelerated warm-up, but the model well predicts the influence of warm gas convection close to the boundary with respect to the conduction along the valve stem, for example when the temperature trend inverts at t~1800s.

6. Conclusions and Future Perspectives

The present activity's main goal was to characterize the liquid nitrogen flow inside an industrial valve at cryogenic conditions both experimentally and numerically, highlighting the occurrence of cavitation through the valve. A conventional cryogenic ball valve has been selected to perform this study due to its wide range of application in different sectors. The experimental data has been processed to retrieve the global parameters such as flow coefficient K_v and liquid recovery factor F_L. Flow visualization has been performed both upstream and downstream of the tested valve, confirming the existence (or not) of two-phase flow conditions. At cavitation conditions, a bubbly flow is visualized which propagates further downstream of the valve outlet. Numerical results of mass flow rate show a good agreement against available experimental data, although the liquid recovery factor exhibits some discrepancies which are not yet fully understood. Moreover, the definition of downstream pressure boundary condition below the liquid saturation pressure leads to the generation of large amounts of vapor which are not found experimentally. Both energy conservation considerations and fluid compressibility need to be considered to properly resolve the challenging cryogenic cavitating flow.

Contextually to the hydraulic performance investigation, the valve stem temperature history at different locations was monitored during the experimental tests. It has been shown that the driving heat transfer mechanism is conduction through the valve body. A 1D transient model has been proposed to capture the temperature trend observed in the experimental results. Agreement between experiments and model is within a maximum deviation of 15% at the valve central position.

Acknowledgements

The authors thankfully acknowledge the contribution of L. Peveroni and J.-B. Gouriet for the design of the experimental methodology and the support in the data analysis. The financial support of the CETIM (Centre Technique des Industries Mécaniques) situated in Nantes, France, is gratefully acknowledged.

References

[1] Handbook for Control Valve Sizing, 2008, https://www.parcol.com/docs/ACA0101_gb.pdf
[2] IEC 60534-2-3, Industrial process control valves, Part 2-3: Flow Capacity - Test Procedure, Second edition 1997.
[3] Stiles, G., “Cavitation and flashing considerations”, in ISA Handbook of Control Valves, Ed. J.W. Hutchinson, 1976, pp.206-211
[4] J. Pinho, J, (2019). “Experimental and numerical study of a cryogenic valve using liquid nitrogen and water”, Aerospace Science and Technology, 93, 105331, 2019.
[5] Esposito, C., “Void Fraction and Speed of Sound Measurement in Cavitating Flows by the Three Pressure Transducers (3PT) Technique”, Exp. Th. Fl. Sci. (112), p. 109949, 2020.
[6] Schnerr G.H., “Physical and numerical modeling of unsteady cavitation dynamics”, in: Fourth International Conference on Multiphase Flow Proceeding, ICMF New Orleans, 2001.
[7] Fontanarosa D, “Implementation and validation of an extended Schnerr-Sauer cavitation model for non-isothermal flows in OpenFOAM” Energy Procedia, vol 126, pp. 58-65, 2017.
[8] A. Bejan, “Heat Tranfser,” Ed. New York: Wiley, 1993, pp. 311-312.